Nanoscale Res Lett (2010) 5:1561–1569
DOI 10.1007/s11671-010-9677-z

NANO EXPRESS

Characterisation and Skin Distribution of Lecithin-Based Coenzyme Q10-Loaded Lipid Nanocapsules

Huafeng Zhou · Yang Yue · Guanlan Liu · Yan Li · Jing Zhang · Zemin Yan · Mingxing Duan

Received: 10 March 2010 / Accepted: 29 June 2010 / Published online: 20 July 2010
© The Author(s) 2010. This article is published with open access at Springerlink.com

Abstract The purpose of this study was to investigate the influence of the inner lipid ratio on the physicochemical properties and skin targeting of surfactant-free lecithin-based coenzyme Q10-loaded lipid nanocapsules (CoQ10-LNCs). The smaller particle size of CoQ10-LNCs was achieved by high pressure and a lower ratio of CoQ10/GTCC (Caprylic/capric triglyceride); however, the zeta potential of CoQ10-LNCs was above /− 60 mV/ with no distinct difference among them at different ratios of CoQ10/GTCC. Both the crystallisation point and the index decreased with the decreasing ratio of CoQ10/GTCC and smaller particle size; interestingly, the supercooled state of CoQ10-LNCs was observed at particle size below about 200 nm, as verified by differential scanning calorimetry (DSC) in one heating–cooling cycle. The lecithin monolayer sphere structure of CoQ10-LNCs was investigated by cryogenic transmission electron microscopy (Cryo-TEM). The skin penetration results revealed that the distribution of Nile red-loaded CoQ10-LNCs depended on the ratio of inner CoQ10/GTCC; moreover, epidermal targeting and superficial dermal targeting were achieved by the CoQ10-LNCs application. The highest fluorescence response was observed at a ratio of inner CoQ10/GTCC of 1:1. These observations suggest that lecithin-based LNCs could be used as a promising topical delivery vehicle for lipophilic compounds.

H. Zhou · Y. Yue · G. Liu · Y. Li · J. Zhang · M. Duan (✉)
State-key Laboratory of Biomembrane and Membrane Biotechnology, School of Life Sciences, Tsinghua University, 100084 Beijing, China
e-mail: duanmx@mail.tsinghua.edu.cn

H. Zhou · Z. Yan
Jiangsu Longliqi Bioscience Co., Ltd., 215555 Suzhou, China
e-mail: zhfforever@yahoo.com.cn

Keywords Coenzyme Q10 · Cryo-TEM · DSC · Topical delivery · Lipid nanocapsules

Introduction

Coenzyme Q10 (CoQ10), a vitamin-like substance with a yellow-coloured crystalline powder form and the melting point of 49°C, is widely biosynthesised in living organisms such as plants and animals [1]. It has been found in virtually all cells of the human body, including the heart, liver and skeletal muscles [2]. Initially, it became a popular supplement due to participation in two major physiological activities: as a mitochondrial electron-transporter in the high-energy metabolic pathways of liver cells and other cells of the body and as an antioxidant against free radicals and lipid peroxidation [3–5]. Recently, CoQ10, as a cutaneous antioxidant and energiser, had been demonstrated to prevent photoaging in topical application. It not only penetrates into the viable epidermis and reduces the level of oxidation and wrinkle depth but also reduces the detrimental effects of ultraviolet A (UVA) on dermal fibroblasts, which maintain the dermal matrix. To be able to act as a cutaneous antioxidant and energiser, CoQ10 needs to penetrate into the above living layers [6, 7].

However, stratum corneum acts as an effective barrier to many compounds [8, 9]. Regarding the skin barrier, several delivery carriers, such as solid lipid nanoparticles (SLN) [10–12], nanostructured lipid carriers (NLC) [13–15], nanoemulsions (NE) [16, 17], microemulsions [18, 19], liposomes [20, 21] and niosomes [22, 23], have been developed and focused on drug absorption and targeting. NLC formulation has been proven to be a suitable colloidal carrier for epidermal targeting, and the degree of

epidermal targeting depended on the oil content and the occlusion factor [24]. It was reported that, following SLN dispersion, dye penetration increased by about fourfold over the uptake obtained following cream application. NLC proved to be less potent (less than threefold increase), and penetration even appeared reduced when applying an NE [25]. Podophyllotoxin-loaded SLN, stabilised by 1.5% soybean lecithin and 0.5% poloxamer 188, provided a good epidermal targeting effect [26]. Interestingly, lecithin microemulsion has shown the highest deposition of fluorescent dye in the dermis layer as the time of treatment increased due to the presence of lecithin [27], but has shown no significant difference in the epidermis layer. Recently, lipid nanocapsules, a medium-chain triglyceride core surrounded by a membrane made from a mixture of lecithin and a PEGylated surfactant, were invented based on the above delivery carrier systems as an intravenous delivery system for application of lipophilic drugs. The lipid nanocapsules were prepared by phase-inversion temperature method. The selection of surfactant and the preparation temperature were the key factors and were difficult to control. The relative amount of surfactant to lipid core content had potential cytotoxicity. However, tissue targeting of lipid nanocapsules was investigated [28–33].

In this study, aimed to establish a delivery system that can target CoQ10 to the dermis layer and the epidermis layer, surfactant-free CoQ10-loaded lipid nanocapsules (CoQ10-LNCs), composed of the lamellar shell of lecithin and an inner lipid core of CoQ10 and GTCC, were developed by high-pressure homogenisation at a high temperature. Varying ratio of CoQ10/GTCC, CoQ10-LNC physicochemical properties, particle size and zeta potential, degree of crystallisation and micromorphology structure were investigated. Furthermore, targeting of CoQ10-LNCs was determined on rat skin in vivo using Nile red as the fluorescence model.

Materials and Method

Materials

Soybean lecithin was purchased from Cargill Texturizing Solutions Deutschland GmbH & Co. KG. (Germany), CoQ10 was purchased from Zhejiang Medicine Co. Ltd., Xinchang Pharmaceutical Factory (China), Nile red (NR) was obtained from Sigma–Aldrich (USA). 2-Propanol and optimal cutting temperature compound (OCT) were purchased from Leica Microsystem (Germany). Caprylic/capric triglyceride (GTCC) was provided by Croda Co. Ltd. (UK).Glycerol, ethane and hexane were reagent grade.

Preparation of CoQ10-Loaded Lipid Nanocapsules

CoQ10-LNCs were prepared according to the process described by Huynh et al. [28], including several changes. The content of CoQ10 was varied from 100% (w/w) to 0% (w/w) in the lipid (CoQ10 and GTCC), and the amount of lipid (CoQ10 and GTCC) was kept at a fixed concentration of 12.5% (w/w) with regard to the total mass of 100 g. Briefly, CoQ10 and GTCC were mixed at 60°C, and then 5% (w/w) lecithin was dissolved into. Next, the above liquid lipid phase was dispersed in 82.5% (w/w) glycerol aqueous solution (glycerol concentration was 40% (w/w)) at 60°C and emulsified by a stirrer at 1500 rpm for 1 min. Lastly, the resulting pre-emulsion was homogenised by high-pressure homogenisation (HPH, NS1001L, Niro Soavi, Italy) at 60°C for 3 cycles at 300 bar, 600 bar and 1000 bar, respectively. The resulting dispersion was cooled at ambient conditions to room temperature to obtain the CoQ10-LNCs.

Particle Size Analysis

The mean particle size (MPZ) was analysed by photon correlation spectroscopy (PCS) using a Malvern Zetasizer 2000 (Malvern Instruments, UK). The MPZ was obtained by averaging three measurements at an angle of 90° in 1-cm diameter cells at 25°C. All of the samples were diluted with distilled water about 50 times.

Zeta Potential Analysis

Malvern Zetasizer 2000 was used to measure the zeta potential (ZP) of CoQ10-LNCs. The value of ZP was obtained by averaging three measurements at 25°C. All the samples were diluted with distilled water about 200 times.

Differential Scanning Calorimetry

Differential scanning calorimetry (DSC) was measured on a DSC Q2000 apparatus (TA Instruments, USA). About 10 mg of each sample was sealed in a 40-μl aluminium pan. Heating was performed from −60°C to 60°C at a heating rate of 5°C/min, and cooling was performed from 60°C to −60°C at a cooling rate of 5°C/min. An empty aluminium pan was used as a reference. The crystalline index (CI [%]) was calculated by applying the following equation:

$$\mathrm{CI}[\%] = \left(\frac{\Delta H_{\mathrm{LNCs}}}{\Delta H_{\mathrm{Bulk\ material}} \times \mathrm{Concentration}_{\mathrm{Lipid}}}\right) \times 100 \quad (1)$$

where, ΔH represents the melting enthalpy (J/g).

Cryogenic Transmission Electron Microscopy (Cryo-TEM)

In this experiment, all the samples were diluted with distilled water about five times. For Cryo-TEM, 4 μl of sample were applied onto a perforated carbon film grid (R1.2/1.3 Quantifoil Micro Tools GmbH, Jena, Germany) and were blotted by filter paper (Whatman 1 μ) for about 3 s. After blotting, the grid was immediately plunged into pre-cooled liquid ethane for flash freezing. The Cryo-grid was held in a Gatan 626 cryo-holder (Gatan, USA) and transferred into TEM (JEOL JEM-2010 with 200 kV LaB6 filament) at −172°C. The sample was observed under minimal dose condition at −172°C. The micrographs were recorded by a Gatan 832 CCD camera at a magnification of 10,000–50,000 × and at a defocus of 3–5.46 μm.

Skin Permeation Studies in vivo

Treatment of Animals

Fifteen ten-week-old female SD rats (200–250 g, Vitalriver Inc., Beijing, China), in similar development stages, were selected as the animal model. They were anaesthetised by a suitable dose of barbital sodium throughout the entire experiment. The fur on the abdominal area of the rats was carefully removed by an electrical shaver to avoid damage to their stratum corneum. The furless abdominal area was used for in vivo transport studies.

Transport Studies

For each set of experiments, 50 mg of sample was well distributed on the hairless abdominal skin area of approximately 3.14 cm^2. At a fixed time after application, surplus sample was removed from the skin surface, and the skin surface was washed three times with PBS and dried gently under cold wind with an electric hair drier. A 0.5 cm × 0.5 cm skin piece was cut out from the treated area, embedded in OCT and frozen rapidly by liquid nitrogen. The specimen, taken out from liquid nitrogen, was frozen on a metal block. The metal block was then transferred into a cryostat microtome (LE ICACM 1850, Germany) for slicing the vertical cross-sections of skin. Twelve vertical skin sections with a thickness of 25 μm were obtained and stored at 4°C until microscopy analysis.

Fluorescent Microscopy

Skin sections were subjected to fluorescent microscopy using an Olympus CK40 microscope (Olympus, Japan) equipped with a UV source and a filter for fluorescent measurement. Image capture and analysis were carried out by Image-pro plus software (Media Cybernetics, USA). The excitation and emission wavelengths were 549 and 628 nm for NR. We selected green light and red light as excitation and emission ranges, respectively. Images were recorded by setting the camera integration time to 1/1.8 s. The same parameters were used for imaging all samples. Fluorescence intensity values were quantified using Image-pro plus software.

Data Analysis

All the data tests were repeated three times and expressed as the mean ± SD. The statistical data were analysed by *t*-test analysis via Origin 7.0; $p < 0.01$ was considered to be statistically significant.

Results and Discussion

Particle Size and Zeta Potential of CoQ10-LNCs

Table 1 shows the MPZ of CoQ10-LNCs evaluated by Zetasizer 2000 after production at different homogenisation pressures. At the homogenisation pressure of 300 bar, MPZ of CoQ10-LNCs was in the range of 290–420 nm; when the pressure reached 600 bar, the MPZ of CoQ10-LNCs was between 200 and 140 nm; when the pressure was raised to 1000 bar, the MPZ of CoQ10-LNCs was from 100 to 70 nm. MPZ of CoQ10-LNCs declined with decreasing CoQ10 content in the lipid phase. Several factors, e.g., type and concentration of lipids and surfactants [34], the viscosity of the lipid phase [24] and homogenisation pressure and cycle time [35], affected the mean particle size of LNCs. During the production process of CoQ10-loaded LNCs, the lipid phase was heated up to 60°C and the viscosity of the lipid phase, dependent on the content of CoQ10, declined with decreasing concentration of CoQ10, similarly to previously described evaluation [36].

The zeta potential characterises the surface charge of the particles, gives information about repulsive forces between particles or droplets and makes a prediction about the stability of colloid dispersions. An absolute value above 30 mV usually indicates good stability of the colloid dispersion [37]. The ZP of the CoQ10-LNCs is shown in Table 2. All developed LNCs displayed a negative charge, and the highest ZP value was above −60 mV, indicating good physical stability of LNCs (data not shown). The CoQ10-loaded LNCs displayed similar ZP values (−64.5, −66.2, −65.3 and −65.5 mV for different CoQ10 loadings) with no significant difference, while the LNCs free of CoQ10 had a lower ZP value (−62.2 mV). However, the LNCs free of lipid phase had the lowest ZP value of about

Table 1 Mean particle size (MPZ) of CoQ10-LNCs after being produced for three cycles at 300 bar/600 bar/1000 bar, respectively ($n = 3$)

Formulation	Lipid content		MPZ (nm)		
	CoQ10 (w/w %)	GTCC (w/w %)	300 bar	600 bar	1000 bar
CoQ10-LNCs-100	100	0	414 ± 15	192 ± 3	98 ± 6
CoQ10-LNCs-75	75	25	343 ± 16	181 ± 6	82 ± 8
CoQ10-LNCs-50	50	50	313 ± 9	174 ± 2	78 ± 5
CoQ10-LNCs-25	25	75	317 ± 4	175 ± 9	76 ± 3
CoQ10-LNCs-0	0	100	298 ± 2	141 ± 4	71 ± 11

Table 2 Zeta potential (ZP) of CoQ10-LNCs analysed by Zetasizer 2000 after being homogenised at 1000 bar for three cycles ($n = 3$)

Formulation	ZP (mV)
CoQ10-LNCs-100	−64.5 ± 0.8
CoQ10-LNCs-75	−66.2 ± 1.1
CoQ10-LNCs-50	−65.3 ± 0.5
CoQ10-LNCs-25	−65.5 ± 1.8
CoQ10-LNCs-0	−62.2 ± 1.2

−49.2 mV (data not shown). Because GTCC has carboxylic groups with negative charges and CoQ10 possesses carbonyl groups and a double-bond group with negative charges, when the lipid CoQ10 and GTCC were incorporated into the LNCs, CoQ10-loaded LNCs demonstrated higher ZP value.

DSC Investigation

Figure 1 shows the DSC curves of CoQ10, GTCC and CoQ10-LNCs recorded from −60°C to 60°C at a heating rate of 5°C/min and cooled from 60°C to −60°C at a rate of 5°C/min. Table 3 shows the DSC parameters of the above developed sample. Compared to bulk CoQ10, the CoQ10-LNC dispersions without any homogenisation process showed a melting peak indicating a solid state. Both melting point and CI of CoQ10 in the formulation decreased with decreasing ratio CoQ10/GTCC from 100% CoQ10 to 25% CoQ10; conversely, the peaks broadened. The melting point of CoQ10 decreased from 48.11°C (CoQ10-NLCs-100-0 bar) to 34.41°C (CoQ10-NLCs-25-0 bar), and CI% declined from 95.77 to 68.91% due to the addition of liquid GTCC. Furthermore, the CoQ10-loaded LNC dispersions (290–420 nm), homogenisation at 300 bar for 3 cycles, showed a weak peak, and the melting point of CoQ10 decreased by slightly less than 1°C in the formulation with the same component, but the CI% greatly decreased (from 95.77 to 1.94%, from 85.06 to 2.24%, from 77.56 to 2.52% and from 68.91 to 2.78% for different formulations). However, when the homogenisation pressure reached 600 bar, resulting in a smaller size of 200–140 nm, the melting point of CoQ10 was absent from the heating DSC curves, indicating no heating enthalpy change and a high likelihood of a supercooled state. The decrease of melting point and CI and the presence of supercooled state were explained by the effect of the nanometre particle size with higher specific surface area. Attributed to the Kelvin effect described by the Thomson equation [38–40], the nanosize effect delays or avoids the recrystallisation of CoQ10 matrix. Additionally, the decrease of the melting point is also affect by surfactants [39]. From the above results, it was determined that CoQ10 loaded in the LNCs was likely in the supercooled state when the particle size of CoQ10-LNCs reached or dropped below 200 nm.

Compared to bulk GTCC, the formulations without any homogenisation showed a melting peak. Both melting point and CI of GTCC in the formulation decreased with decreasing concentration of GTCC. When the homogenisation pressure was 300 bars, the melting point of GTCC decreased by large amounts for changes in the formulation with the same composition, excluded the formulation CoQ10-LNCs-75 (25% GTCC). The same phenomena were observed at 600 bars. However, the melting point of GTCC is absent in the formulation CoQ10-LNCs-75. Interestingly, when the homogenisation pressure was 1000 bar, the DSC parameters were similar to the ones at 600 bars.

On the cooling curves, without any homogenisation pressure, the crystallisation point of GTCC declined from −44.34 (100% GTCC) to −49.9°C (75% GTCC). When the concentration of GTCC decreased to 50%, the crystallisation point decreased to below −60°C, the possible reason being that CoQ10 molecule entered into the structure of GTCC and disturbed the ordered structure of GTCC [41]. When the concentration of CoQ10 increased to 25%, one broadened crystallisation peak at about −35°C was present on the cooling curves, possibly representing the co-melting complex of GTCC/CoQ10. When the concentration of CoQ10 increased to 50%, one narrow crystallisation peak (−30.89°C) and two weak crystallisation peaks (−22.75 and −10.08°C) were present. When the concentration of CoQ10 increased to 75%, one relatively narrow crystallisation peak (−31.21°C) and one broadened strong peak (−9.28°C) was shown on the cooling curves. Compared to pure CoQ10 (0% GTCC), the depression of the crystallisation point of CoQ10 may be explained by the

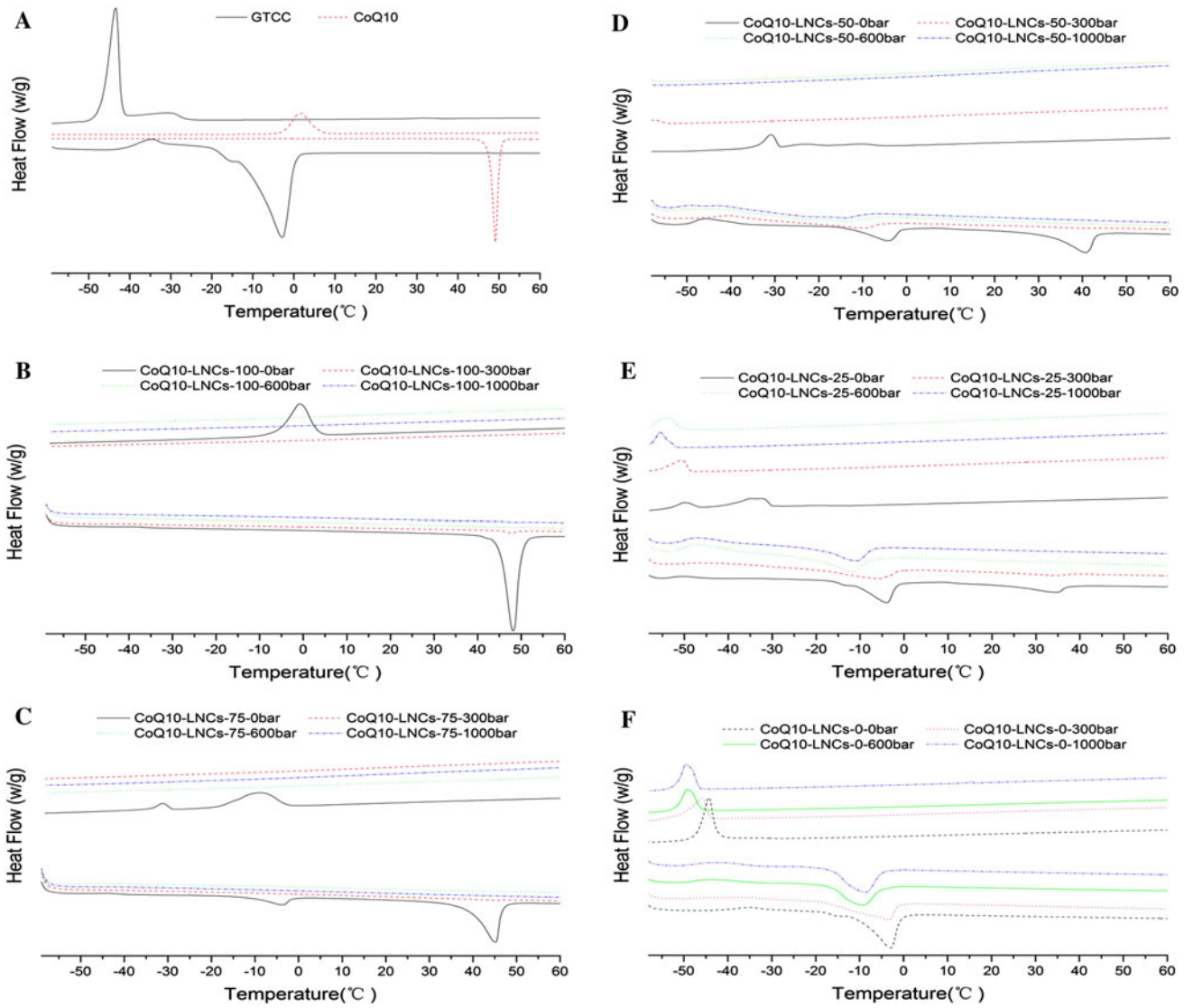

Fig. 1 DSC heating and cooling curves of bulk materials and CoQ10-LNCS from −60°C to 60°C at a heating rate 5°C/min and cooled from 60°C to −60°C at a rate 5°C/min. **a** bulk material GTCC and CoQ10; **b** CoQ10-LNCs-100 prepared at 0 bar, 300 bar, 600 bar and 1000 bar; **c** CoQ10-LNCs-75 prepared at 0 bar, 300 bar, 600 bar and 1000 bar; **d** CoQ10-LNCs-50 prepared at 0 bar, 300 bar, 600 bar and 1000 bar; **e** CoQ10-LNCs-25 prepared at 0 bar, 300 bar, 600 bar and 1000 bar; and **f** CoQ10-LNCs-0 prepared at 0 bar, 300 bar, 600 bar and 1000 bar

GTCC molecule entering into the structure of CoQ10 resulted in less ordered crystal structure of CoQ10 during the cooling process [10], delaying the crystallisation point. However, after high-pressure homogenisation (above 300 bar), the crystallisation peaks of CoQ10 and of the co-melting complex of GTCC/CoQ10 were absent, indicating a supercooled state due to the effect of nanosize particles. From the above result, the crystallisation point of CoQ10-LNCs depended mainly on the size of the particles; when the size reached down to about 200 nm, no crystallisation of CoQ10 was present, indicating supercooled state. Supercooled nanoparticles were potentially more stable with respect to nanoparticles recrystallisation over other types of lipid nanoparticles like fat emulsions and solid lipid nanoparticles [42].

Cryo-TEM Investigation

The advantage of Cryo-TEM is that the liquid dispersion can be frozen and viewed directly in the frozen state; thus, the samples are investigated close to their natural state [43–46]. The morphology of the LNC structures was investigated with the composition varying in weight ratio of CoQ10/GTCC (100, 75, 50, 25 and 0% CoQ10), homogenised at 1000 bar for three cycles. Cryo-TEM images of the above LNC dispersions, diluted with water five times, are

Table 3 DSC parameters of GTCC and CoQ10 in the bulk GTCC, CoQ10 and CoQ10-LNCs 3 days after being produced for three cycles at 300 bar/600 bar/1000 bar, respectively

Formulation	GTCC				CoQ10			
	Melting point (°C)	Onset (°C)	Enthalpy (J/g)	CI%	Melting point (°C)	Onset (°C)	Enthalpy (J/g)	CI%
GTCC	−2.92	−11.57	95.63	100	/	/	/	/
CoQ10	/	/	/	/	49.12	47.76	131.2	100
100-0 bar	/	/	/	/	48.11	45.19	16.75	95.77
100-300 bar	/	/	/	/	47.84	45.53	0.3388	1.94
75-0 bar	−3.69	−10.29	2.21	69.27	45.16	39.41	11.16	85.06
75-300 bar	/	/	/	/	44.72	38.94	0.2943	2.24
50-0 bar	−4.03	−12.53	4.29	67.32	40.72	32.61	6.787	77.56
50-300 bar	−11	−35.19	4.19	65.67	39.54	31.93	0.2208	2.52
50-600 bar	−23.05	−40.19	4.03	63.18	/	/	/	/
50-1000 bar	−23.2	−40.76	4.09	64.12	/	/	/	/
25-0 bar	−4.08	−11.96	8.57	89.61	34.41	26.35	3.011	68.91
25-300 bar	−6.11	−29.92	6.63	69.29	34.44	26.15	0.1216	2.78
25-600 bar	−11.92	−19.84	5.39	56.37	/	/	/	/
25-1000 bar	−11.61	−19.73	5.38	56.31	/	/	/	/
0-0 bar	−3.05	−10.18	12.01	94.21	/	/	/	/
0-300 bar	−3.44	−18.24	9.69	75.99	/	/	/	/
0-600 bar	−9.23	−16.35	9.28	72.78	/	/	/	/
0-1000 bar	−8.69	−16.12	9.17	71.67	/	/	/	/

shown in Fig. 2. The bilayer of unilamellar structure (Fig. 2F-b) and monolayer of unilamellar structure (Fig. 2F-a) were present in the spherical shape; the thickness of the bilayer and monolayer was about 5 and 2 nm, respectively. Interestingly, one novel double-sphere structure (Fig. 2F-c), one bilayer sphere and one monolayer sphere were discovered. In all five formulations (from Fig. 2A to E), the monolayer structure spheres were predominant, and the independent bilayer structure spheres were a very small minority, replaced by the double-sphere structure. The ratio of CoQ10/GTCC affected the distribution of the double-sphere structure; when the GTCC content was dominant, the double-sphere structure was rare. Several lipid microstructures, for example, bilayer, monolayer, multilamellar, were reported, determined by Cryo-TEM [43–46]. The monolayer of unilamellar structure with the background inner core, compared to the outer environment, showed the lipid core, while the bilayer of unilamellar structure with the same inner core background, compared to the outer environment, showed no loading in the core.

Skin Penetration Study

NR, a selective fluorescent stain for intracellular lipid droplets, has been used to visualise the skin penetration study successfully [47, 48]. To investigate the effect of LNCs with varying ratio of CoQ10/GTCC as a topical delivery vehicle, NR (2.5 μg/ml) was used as fluorescent dye model incorporated into the lipid phase during this procedure. Five formulations, with composition shown in Table 1, were homogenised at 1000 bar for three cycles and used in this study. The rat skin without any treatment was used as the control. Figure 3 shows the fluorescence images of vertical skin section of rats, having applied the NR-loaded CoQ10-LNCs for 3 h. In Fig. 3f, fluorescence response from the epidermis and hair follicle was observed at the excitation and emission wavelength, contributed by autofluorescence; however, almost no fluorescence signal was detected in the dermis area. After treatment with CoQ10-LNCs, there was obvious fluorescence, with different distributions depending on the ratio of CoQ10/GTCC, and the fluorescence signals of the epidermis and hair follicle were stronger. When the ratio of CoQ10/GTCC was 1:1, the fluorescence response of the epidermis was the strongest, with the decline of the fluorescence signal for CoQ10-LNCs-25 and CoQ10-LNCs-0, while the fluorescence response of the hair follicle became stronger with increasing content of GTCC. Interestingly, a strong fluorescence signal of the superficial dermis was observed, and the LNCs with a lower ratio of CoQ10/GTCC showed higher intensity of fluorescence in the superficial dermis area. When the ratio of CoQ10/GTCC was decreased to 1:1 (CoQ10-LNCs-50), the intensity of fluorescence of the superficial dermis was the strongest, with decreasing fluorescence signal for CoQ10-LNCs-25 and CoQ10-LNCs-0. The superficial

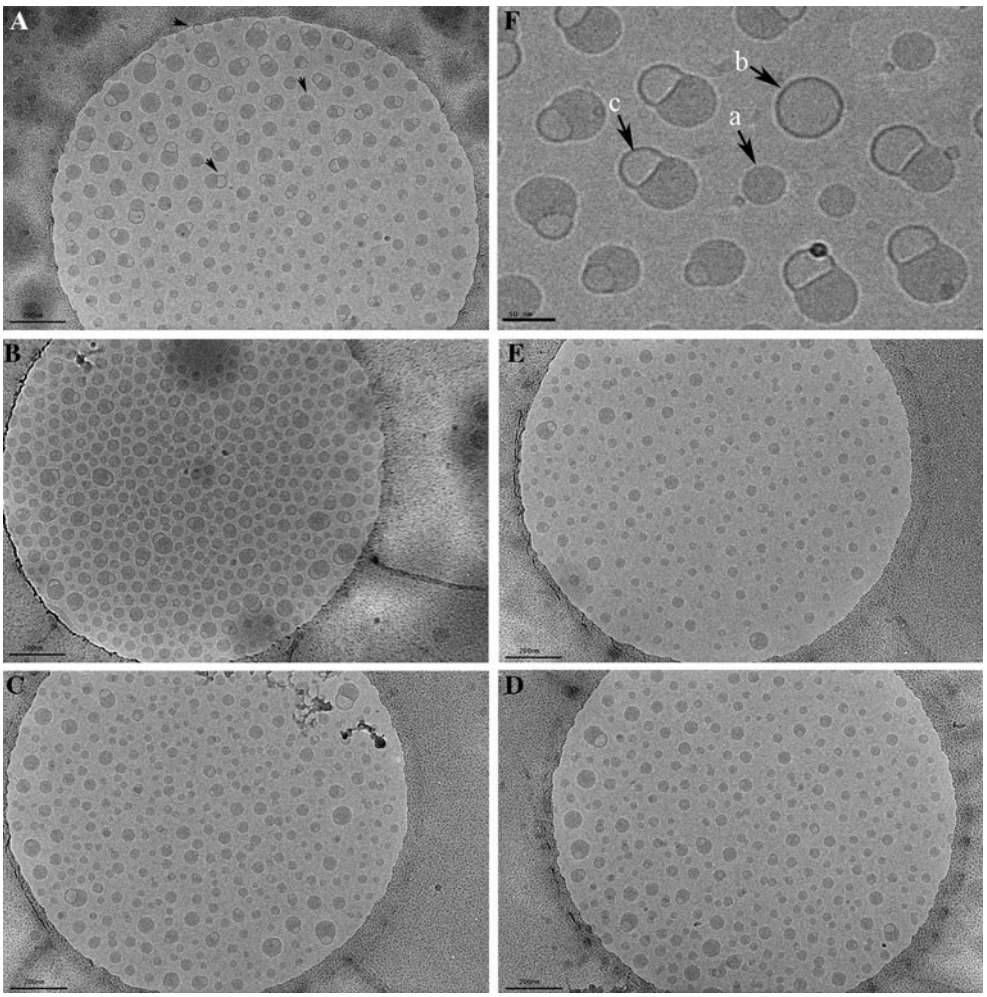

Fig. 2 Microstructure obtained by Cryo-TEM of CoQ10-LNCs at a magnification of 15000 with different contents of CoQ10 in the inner lipid core, prepared at a pressure of 1000 bar. **A** CoQ10-LNCs-100; **B** CoQ10-LNCs-75; **C** CoQ10-LNCs-50; **D** CoQ10-LNCs-25; **E** CoQ10-LNCs-0; and **F** CoQ10-LNCs-100, photo at a magnification of 50000

dermis skin fluorescence measurement of NR is expressed in arbitrary units (ABU), and quantitative analysis of dye penetration was obtained from pixel intensities derived from fluorescence measurements of the skin slices (Fig. 4). However, weak or no fluorescence response was observed in the lower dermis. Similar results have been previously reported. Improving the uptake and skin targeting may become feasible by means of nanoparticular systems such as solid lipid nanoparticles (SLN), NLC and NE [25]; NLC revealed higher epidermal drug targeting, and the dye distribution depended on the MCT content of the NLC [24]; podophyllotoxin-loaded SLN provided good epidermal targeting [26]. From the above results, LNCs showed not only good superficial dermis targeting but also good epidermis targeting, indicated by the strong intensity of fluorescence; the degree of fluorescence response depended on the ratio of CoQ10/GTCC.

The significant extent of skin penetration was most likely attributed to the fact that nanoparticles provided superior skin hydration, which was helpful for improving the permeation effect [49]. Assuming that the average width of transepidermal hydrophilic pathway is up to about 100 nm as the intercorneocyte space, it is conceivable for nanosize particles to traverse through the intercorneocyte spaces [50, 51]. Moreover, an increase in penetration extent may result from an alteration in the barrier properties and a greater degree of partitioning of the LNCs into the stratum corneum and was closely related to the nature of surfactant [52]. Previous investigations on the mechanism of transdermal permeation of phospholipid microemulsion indicate that phospholipids mainly increased the fluidity of the intercellular lipids of the stratum corneum, which led to enhancement of percutaneous permeation of drugs [49, 53].

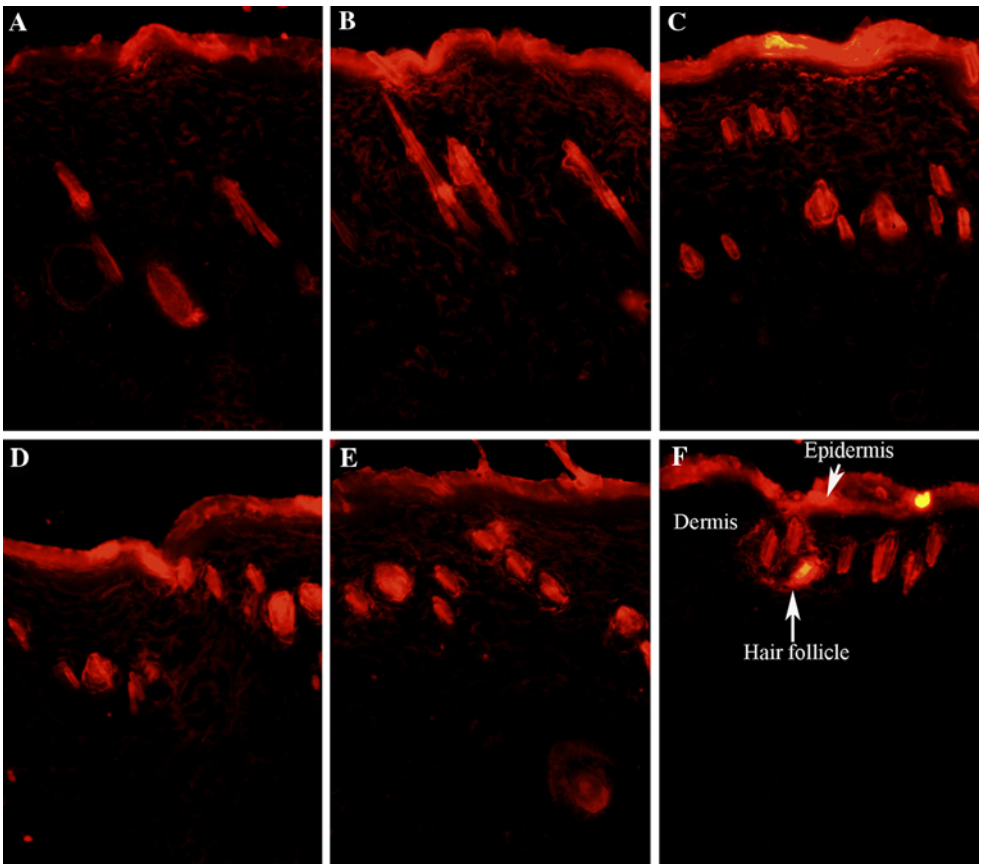

Fig. 3 Fluorescent images of skin slices treated with NR-loaded CoQ10-LNCs (2.5 μg/ml) for NR dye for about 3 h. **a** Fluorescent images of skin slices applied with CoQ10-LNCs-100; **b** fluorescent images of skin slices applied with CoQ10-LNCs-75; **c** fluorescent images of skin slices applied with CoQ10-LNCs-50; **d** fluorescent images of skin slices applied with CoQ10-LNCs-25; **e** fluorescent images of skin slices applied with CoQ10-LNCs-0; and **f** fluorescent images of skin slices without of any application of CoQ10-LNCs

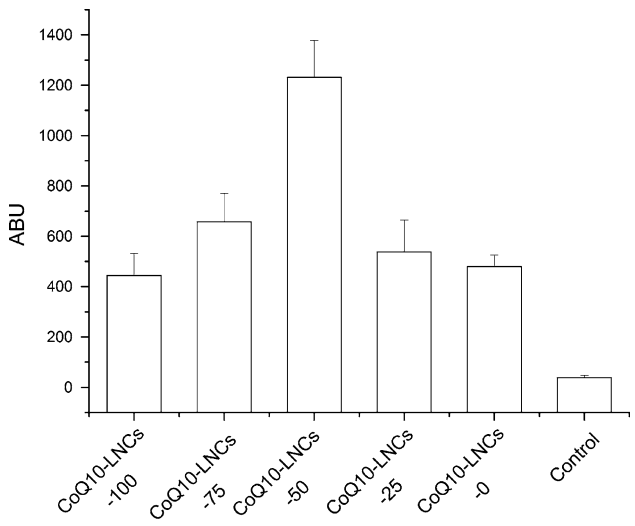

Fig. 4 Fluorescent ABU values of superficial dermis layer treated with NR-loaded CoQ10-LNCs (2.5 μg/ml) for about 3 h

Conclusion

Surfactant-free CoQ10-LNCs, composed of lecithin, CoQ10 and GTCC, were successfully prepared by high-pressure homogenisation. Particle size was the primary influencing factor on the CI of CoQ10, while the ratio of CoQ10/GTCC was the key factor affecting the crystallisation point of CoQ10. When the particle size of CoQ10-LNCs reached about 400 nm, the CI of CoQ10 was reduced to less than 3%; when the size further decreased to about 200 nm, no enthalpy was present. From the cooling process, the supercooled state of CoQ10 was maintained even at a lower temperature (−40°C). The lecithin monolayer structure of CoQ10-LNCs was investigated via the Cryo-TEM method. CoQ10-LNCs structured with a lecithin monolayer sphere have been investigated to be a suitable delivery system for both epidermal targeting and superficial dermal targeting; moreover, the degree of distribution depended on the ratio of CoQ10/GTCC.

Acknowledgments The authors are grateful for Cryo-TEM support by Qinfen Zhang from BioEM lab, State Key Lab of Biocontrol, School of life Sciences, Sun Yat-Sen Universtity, Guangzhou, 510275.

Open Access This article is distributed under the terms of the Creative Commons Attribution Noncommercial License which permits any noncommercial use, distribution, and reproduction in any medium, provided the original author(s) and source are credited.

References

1. H. Nohl, L. Gille, K. Staniek, Ann. N. Y. Acad. Sci. **854**, 394 (1998). doi:10.1111/j.1749-6632.1998.tb09919.x
2. F. Aberg, E. Appelkvist, G. Dallner, L. Ernster, Arch. Biochem. Biophys. **295**, 230 (1992). doi:10.1016/0003-9861(92)90511-T
3. G. Lenaz, R. Fato, C. Castelluccio, M. Cavazzoni, E. Estornell, J.F. Huertas, F. Pallotti, G. Parenti Castelli, H. Rauchova, Mol. Aspects Med. **15**, s29 (1994). doi:10.1016/0098-2997(94)90010-8
4. F.L. Crane, J. Am. Coll. Nutr. **20**, 591 (2001)
5. L. Ernster, G. Dallner, Biochim. Biophys. Acta **1271**, 195 (1995). doi:10.1016/0925-4439(95)00028-3
6. U. Hoppe, J. Bergemann, W. Diembeck, J. Ennen, S. Gohla, I. Harris, J. Jacob, J. Kielholz, W. Mei, D. Pollet, D. Schachtschabel, G. Sauermann, V. Schreiner, F. Stab, F. Steckel, Biofactors **9**, 371 (1999). doi:10.1002/biof.5520090238
7. Y. Shindo, E. Witt, D. Han, W. Epstein, L. Packer, J. Invest. Dermatol. **102**, 122 (1994)
8. E. Proksch, J.M. Brandner, J. Jensen, Exp. Dermatol. **17**, 1063 (2008). doi:10.1111/j.1600-0625.2008.00786.x
9. P.W. Wertz, Acta. Derm. Venereol. Suppl. (Stockh) **208**, 7 (2000)
10. V. Jenning, A. Gysler, M. Schafer-Korting, S.H. Gohla, Eur. J. Pharm. Biopharm. **49**, 211 (2000). doi:10.1016/S0939-6411(99)00075-2
11. V. Sanna, E. Gavini, M. Cossu, G. Rassu, P. Giunchedi, J. Pharm. Pharmacol. **59**, 1057 (2007). doi:10.1211/jpp.59.8.0002
12. H.F. Zhou, Q.H. Ma, Q. Xia, Y. Yan, N. Gu, X. Miao, D. Lu, Solid State Phenom. **121–123**, 271 (2007)
13. E.B. Souto, R.H. Muller, Pharmazie **61**, 431 (2006)
14. H.F. Zhou, Q.H. Ma, Y. Ding, Q. Xia, Y.Z. Kuang, X.Z. Hao, N. Gu, Chin. J. Process Eng. **6**, 598 (2006)
15. Q. Xia, A. Saupe, R.H. Mueller, E.B.E.U. Souto, Int. J. Cosmet. Sci. **29**, 473 (2007). doi:10.1111/j.1468-2494.2007.00410.x
16. F. Shakeel, W. Ramadan, M.A. Ahmed, J. Drug Target. **17**, 435 (2009). doi:10.1080/10611860902963021
17. H.F. Zhou, Y. Yue, G.L. Liu, Y. Li, J. Zhang, Q. Gong, Z.M. Yan, M.X. Duan, Nanoscale Res. Lett. **5**, 224 (2010). doi:10.1007/s11671-009-9469-5
18. S. Peltola, R. Saarinen-Savolainen, J. Kiesvaara, T.M. Suhonen, A. Urtti, Int. J. Pharm. **254**, 99 (2003). doi:10.1016/S0378-5173(02)00632-4
19. E. Peira, D. Chirio, M.E. Carlotti, R. Spagnolo, M. Trotta, J. Drug Deliv. Sci. Technol. **19**, 191 (2009)
20. M. Sentjurc, K. Vrhovnik, J. Kristl, J. Control. Release **59**, 87 (1999). doi:10.1016/S0168-3659(98)00181-3
21. M.H. Schmid, H.C. Korting, Crit. Rev. Ther. Drug **11**, 97 (1994)
22. M.J. Choi, H.I. Maibach, Skin Pharmacol. Physiol. **18**, 209 (2005). doi:10.1159/000086666
23. P. Balakrishnana, S. Shanmugam, W.S. Lee, W.M. Lee, J.O. Kim, D.H. Oh, D.D. Kim, J.S. Kim, B.K. Yoo, H.G. Choi, J.S. Woo, C.S. Yong, Int. J. Pharm. **377**, 1 (2009). doi:10.1016/j.ijpharm.2009.04.020
24. V. Teeranachaideekul, P. Boonme, E.B. Souto, R.H. Muller, V.B. Junyaprasert, J. Control. Release **128**, 134 (2008). doi:10.1016/j.jconrel.2008.02.011
25. S. Lombardi Borgia, M. Regehly, R. Sivaramakrishnan, W. Mehnert, H.C. Korting, K. Danker, B. Röder, K.D. Kramer, M. Schäfer-Korting, J. Control. Release **110**, 151 (2005). doi:10.1016/j.jconrel.2005.09.045
26. H. Chen, X. Chang, D. Du, W. Liu, J. Liu, T. Weng, Y. Yang, H. Xu, X. Yang, J. Control. Release **110**, 296 (2006). doi:10.1016/j.jconrel.2005.09.052
27. M. Changez, J. Chander, A.K. Dinda, Colloids Surf. B Biointerfaces **48**, 58 (2006). doi:10.1016/j.colsurfb.2006.01.007
28. N.T. Huynh, C. Passirani, P. Saulnier, J.P. Benoit, Int. J. Pharm. **379**, 201 (2009). doi:10.1016/j.ijpharm.2009.04.026
29. E. Allard, N.T. Huynh, A. Vessieres, P. Pigeon, G. Jaouen, J. Benoit, C. Passirani, Int. J. Pharm. **379**, 317 (2009). doi:10.1016/j.ijpharm.2009.05.031
30. A.B. Dhanikula, N.M. Khalid, S.D. Lee, R. Yeung, V. Risovic, K.M. Wasan, J.C. Leroux, Biomaterials **28**, 1248 (2007). doi:10.1016/j.biomaterials.2006.10.036
31. D. Hoarau, P. Delmas, S. David, E. Roux, J.C. Leroux, Pharm. Res. **21**, 1783 (2004). doi:10.1023/B:PHAM.0000045229.87844.21
32. F. Lacoeuillel, E. Garcion, J.P. Benoit, A. Lamprecht, J. Nanosci. Nanotechnol. **7**, 4612 (2007). doi:10.1166/jnn.2007.006
33. A. Barras, A. Mezzetti, A. Richard, S. Lazzaroni, S. Roux, P. Melnyk, D. Betbeder, N. Monfilliette-Dupont, Int. J. Pharm. **379**, 270 (2009). doi:10.1016/j.ijpharm.2009.05.054
34. F. Han, S. Li, R. Yin, H. Liu, L. Xu, Colloids Surf. Physicochem. Eng. Aspects **315**, 210 (2008). doi:10.1016/j.colsurfa.2007.08.005
35. J. Floury, A. Desrumaux, J. Lardières, Innov. Food Sci. Emerg. Technol. **1**, 127 (2000). doi:10.1016/S1466-8564(00)00012-6
36. F. Hu, S. Jiang, Y. Du, H. Yuan, Y. Ye, S. Zeng, Colloids Surf. B Biointerfaces **45**, 167 (2005). doi:10.1016/j.colsurfb.2005.08.005
37. C. Freitas, R.H. Müller, Int. J. Pharm. **168**, 221 (1998). doi:10.1016/S0378-5173(98)00092-1
38. E. Zimmermann, E.B. Souto, R.H. Muller, Pharmazie **60**, 508 (2005)
39. S.A. Wissing, R.H. Muller, L. Manthei, C. Mayer, Pharm. Res. **21**, 400 (2004). doi:10.1023/B:PHAM.0000019291.36636.c1
40. K. Westesen, H. Bunjes, Int. J. Pharm. **115**, 129 (1995). doi:10.1016/0378-5173(94)00347-8
41. V. Jenning, A.F. Thunemann, S.H. Gohla, Int. J. Pharm. **199**, 167 (2000). doi:10.1016/S0378-5173(00)00378-1
42. V. Kuntsche, M.H.J. Koch, A. Fahr, H. Bunjes, Eur. J. Pharm. Sci. **38**, 238 (2009). doi:10.1016/j.ejps.2009.07.012
43. A. Saupe, K.C. Gordon, T. Rades, Int. J. Pharm. **314**, 56 (2006). doi:10.1016/j.ijpharm.2006.01.022
44. L. Spernath, O. Regev, Y. Levi-Kalisman, S. Magdassi, Colloids Surf. A Physicochem. Eng. Aspects **332**, 19 (2009). doi:10.1016/j.colsurfa.2008.08.026
45. R. Waninge, T. Nylander, M. Paulsson, B. Bergenstahl, Colloids Surf. B Biointerf. **31**, 257 (2003). doi:10.1016/S0927-7765(03)00145-0
46. D.A. Ferreira, M. Bentley, G. Karlsson, K. Edwards, Int. J. Pharm. **310**, 203 (2006). doi:10.1016/j.ijpharm.2005.11.028
47. P. Greenspan, E.P. Mayer, S.D. Fowler, J. Cell Biol. **100**, 965 (1985)
48. R. Alvarez-Roman, A. Naik, Y.N. Kalia, H. Fessi, R.H. Guy, Eur. J. Pharm. Biopharm. **58**, 301 (2004). doi:10.1016/j.ejpb.2004.03.027
49. H.B. Gunt, G.B. Kasting, Eur. J. Pharm. Sci. **32**, 254 (2007). doi:10.1016/j.ejps.2007.07.009
50. B.W. Barry, Eur. J. Pharm. Sci. **14**, 101 (2001). doi:10.1016/S0928-0987(01)00167-1
51. G. Cevc, Adv. Drug Deliv. Rev. **56**, 675 (2004). doi:10.1016/j.addr.2003.10.028
52. B.W. Barry, Nat. Biotechnol. **22**, 165 (2004). doi:10.1038/nbt0204-165
53. F. Dreher, P. Walde, P. Walther, E. Wehrli, J. Control. Release **45**, 131 (1997). doi:10.1016/S0168-3659(96)01559-3